

**Spike latency and response properties of an excitable micropillar laser**F. Selmi,<sup>1</sup> R. Braive,<sup>1,2</sup> G. Beaudoin,<sup>1</sup> I. Sagnes,<sup>1</sup> R. Kuszelewicz,<sup>3</sup> T. Erneux,<sup>4</sup> and S. Barbay<sup>1,\*</sup><sup>1</sup>*Centre de Nanosciences et de Nanotechnologies, CNRS, Univ. Paris-Sud, Université Paris-Saclay, C2N–Marcoussis, 91460 Marcoussis, France*<sup>2</sup>*Université Paris Diderot, 5 rue Thomas-Mann, 75013 Paris, France*<sup>3</sup>*Neurophotonics Laboratory, CNRS/Université Paris Descartes, 45, rue des Saints-Pères, 75270 Paris, France*<sup>4</sup>*Université Libre de Bruxelles, Optique Nonlinéaire Théorique, Campus Plaine C.P. 231, 1050 Bruxelles, Belgium*

(Received 5 August 2016; published 24 October 2016)

We present experimental measurements concerning the response of an excitable micropillar laser with saturable absorber to incoherent as well as coherent perturbations. The excitable response is similar to the behavior of spiking neurons but with much faster time scales. It is accompanied by a subnanosecond nonlinear delay that is measured for different bias pump values. This mechanism provides a natural scheme for encoding the strength of an ultrafast stimulus in the response delay of excitable spikes (temporal coding). Moreover, we demonstrate coherent and incoherent perturbations techniques applied to the micropillar with perturbation thresholds in the range of a few femtojoules. Responses to coherent perturbations assess the cascability of the system. We discuss the physical origin of the responses to single and double perturbations with the help of numerical simulations of the Yamada model and, in particular, unveil possibilities to control the relative refractory period that we recently evidenced in this system. Experimental measurements are compared to both numerical simulations of the Yamada model and analytic expressions obtained in the framework of singular perturbation techniques. This system is thus a good candidate to perform photonic spike processing tasks in the framework of novel neuroinspired computing systems.

DOI: [10.1103/PhysRevE.94.042219](https://doi.org/10.1103/PhysRevE.94.042219)**I. INTRODUCTION**

The generation of short optical pulses is a key ingredient for optical signal processing and signal transmission applications. Interestingly, self-pulsing lasers with saturable absorbers are usually able to operate in the so-called excitable regime [1–4]. This regime occurs when the laser is biased below the self-pulsing laser threshold and is characterized by an all-or-none type of response to an input perturbation. When the perturbation is below a certain threshold (the excitable threshold), no pulse is emitted, whereas when it is greater than this threshold, a calibrated pulse is emitted. Semiconductor lasers with saturable absorbers are known to behave as fast and compact excitable systems [5] since the typical operating time scales are given by the carrier recombination time, usually a few hundreds of picoseconds. This regime may be useful for traditional optical signal processing applications (e.g., logic gates [6]) as well as to build networks for photonics neuromimetic and spike processing operations [7,8] such as spiking pattern recognition [9], self-regenerative memories [10], and coincidence detection [11–13]. In a recent work [14], we demonstrated a fast excitable dynamics with response times of the order of 200 ps in a micropillar laser with integrated saturable absorber and studied the absolute and relative refractory periods. This behavior is analogous to the one found in biological neurons but with time scales faster by more than 6 orders of magnitude. The absolute refractory period is the latency period after one excitable pulse has fired in which it is not possible to trigger another pulse. Less known in optics is the relative refractory period, i.e., the latency period in which the system has not completely recovered

its stationary state but can respond to an input perturbation, though with a reduced response amplitude and with a higher (dynamical) threshold. In biological neurons, this corresponds to the repolarization and hyperpolarization phases of the action potential generation. The characterization of these periods is crucial for signal processing applications based, e.g., on spike-time coding, or for the stable propagation of activity pulses in spatially extended excitable systems [15]. We give here a more detailed account on these results and we present measurements concerning the timing behavior of the system and its ability to respond to incoherent as well as coherent perturbations. The excitable response is accompanied by a nonlinear delay that is measured for different bias pumps. This mechanism provides a natural scheme for excitable spikes to encode the strength of the stimulus in a response delay. Temporal coding based on relative spike latencies has been successfully implemented in several neurocomputational algorithms for vision processing and pattern recognition [16] and has been demonstrated in the vision processing of retinal ganglion cells [17]. It is thus a particularly important feature of a neuromimetic system. We present experimental results on spike latency in our system in Sec. II and discuss in Sec. III the results in relation with numerical and analytical analysis obtained with the Yamada model. In Sec. IV we analyze in detail the relative refractory period and show numerically how, by controlling the recombination rates of carriers in the system, it is possible to modify the response of the micropillar as well as the nature of the refractory period. Moreover, we propose a physical explanation of this behavior in terms of a dynamical excitable threshold. In Sec. V we experimentally demonstrate the coherent perturbation technique on the micropillar and compare its specific response to the one induced by incoherent perturbations. Responses to coherent perturbations assess the cascability of the system, a key property for building

\*sylvain.barbay@lpn.cnrs.fr

networks of excitable units. They also display calibrated response amplitudes that depend weakly on the perturbation strength, in contrast to the incoherent perturbation case. We discuss the physical origin of the peculiar kinds of responses with the help of numerical simulations. Finally, in Sec. VI, we conclude and bring perspectives of this work in the framework of photonic neural processing.

## II. SPIKE LATENCY

The excitable system under study is a micropillar laser with intracavity saturable absorber emitting at 980 nm. The cavity design is based on an original vertical cavity structure [18,19] optimized for optical pumping around 800 nm and room-temperature operation and integrating a saturable absorber (SA) in the active zone. The active zone consists of two InGaAs quantum wells for the gain section and one InGaAs quantum well for the SA section. A 4- $\mu\text{m}$  diameter micropillar is then etched and the micropillar is further coated with a thick SiN layer to prevent oxidization and to improve heat dissipation [14]. The micropillar is pumped cw by a fiber-coupled array of laser diodes and focused onto the sample with a microscope objective. The dynamics is recorded with a 80-ps rise-time avalanche photodiode, amplified by a 18-GHz bandwidth RF amplifier and recorded by a 13-GHz oscilloscope. Optical perturbation pulses, 80 ps in duration, are provided by a mode-locked Ti:Sa laser operating at a repetition rate of 82 MHz whose output rate can be down-converted thanks to an acousto-optic modulator.

The responses to short optical perturbations in the pump window ( $\sim 800\text{nm}$ ) are shown in Fig. 1(a). They display the typical behavior already reported in Ref. [14], i.e., a sharp jump at the excitable threshold and an increase of the excitable threshold for lower pump values. The excitable threshold increase is accompanied with a reduction of the height of the response step, until no more jump is visible as the excitable regime disappears at the benefit of a gain switching regime. These observations have been successfully compared to numerical simulations of the Yamada model with an excellent agreement in Ref. [14]. A dynamical delay between the perturbation and the response occurrences is measured and is plotted in Fig. 1(b). It is obtained by averaging the response delays over 100 perturbation pulses. Its range spans from about 1 ns close to threshold to less than 150 ps away from the excitable threshold. For a given perturbation strength, the delay increases with lower pump values. This latency is exactly similar to the one observed in biological systems [20], except obviously for the time scales at stake: hundreds of picoseconds here versus milliseconds.

## III. NUMERICAL MODELING

We can compare our results to numerical simulations based on the Yamada model [21] with spontaneous emission [4,22]. This model has already shown important properties of the dynamics of semiconductor lasers with SA, and in particular the shape of the curve of excitable response versus perturbation amplitude and its dependence on pumping [14]. It has also been recently recognized [9] as being an optical analog to the leaky integrate-and-fire neuron model in the limit of an infinitely fast

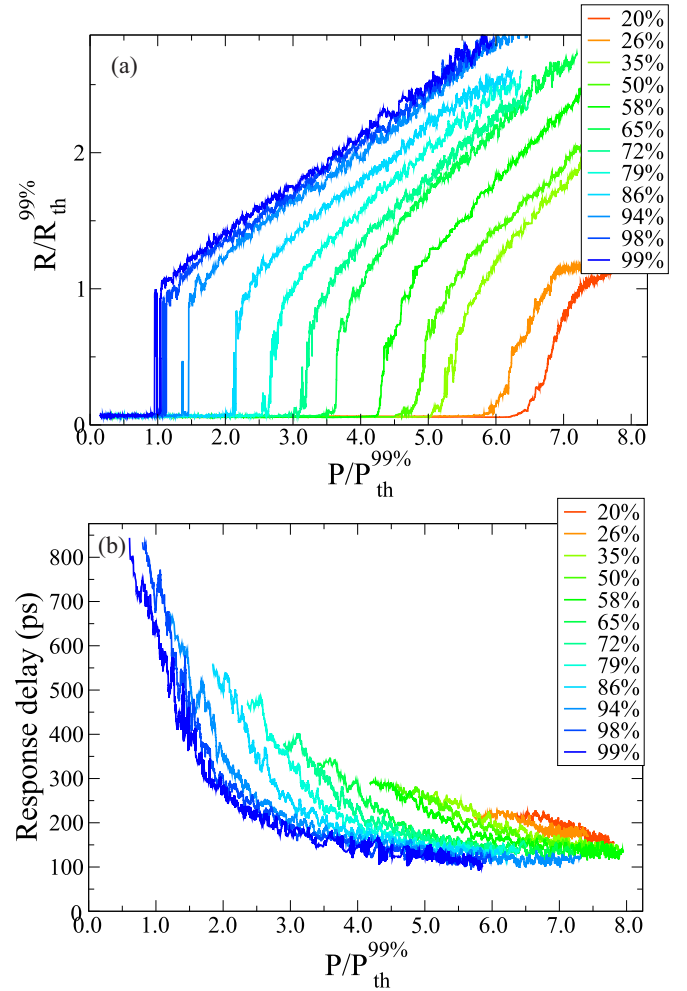


FIG. 1. Median of the response amplitude  $R$  (a) and median of the pulse response delay (b) versus normalized perturbation energy  $P$  for different bias pumps with respect to the self-pulsing pump threshold. The perturbation and the response are normalized respectively to the excitable threshold ( $P_{\text{th}}^{99\%}$ ) and to the response at excitable threshold ( $R_{\text{th}}^{99\%}$ ) for a bias pump  $P$  equal to 99% of the pump at the self-pulsing threshold.

photon cavity lifetime, a model widely used in computational neuroscience [23]. The model reads

$$\begin{aligned} \dot{I} &= I(G - Q - 1) + \beta_{\text{sp}}(G + \eta_1)^2 \\ \dot{G} &= b_1[\mu_1 - G(1 + I)] \\ \dot{Q} &= b_2[\mu_2 - Q(1 + sI)]. \end{aligned} \quad (1)$$

It consists of three coupled nonlinear ordinary differential equations for the intracavity intensity  $I$  and the scaled excess carrier densities with respect to transparency in the gain and in the SA region  $G$  and  $Q$ . Other parameters are  $\mu_1$ , the gain generated through pumping intensity;  $\mu_2$ , the nonsaturable loss;  $s$ , the saturation parameter;  $\beta_{\text{sp}}$ , the spontaneous emission factor; and  $\eta_1$ , the transparency offset of gain. Time is rescaled to the cavity lifetime and  $b_{1,2}$  are the rescaled recombination rates of carriers respectively in the gain and SA regions. We take  $b_1 = 0.001$ ,  $b_2 = 0.002$ ,  $\mu_2 = 2$ ,  $s = 10$ ,  $\eta_1 = 1.6$ ,  $\beta_{\text{sp}} = 10^{-5}$  as parameters suitable for our semiconductor

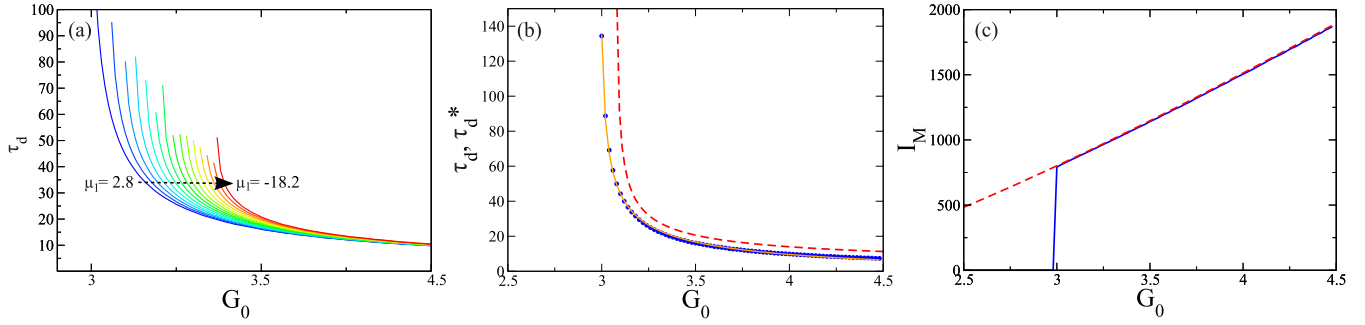


FIG. 2. (a) Response pulse delay  $\tau_d$  from Yamada model with spontaneous emission (full line) versus incoherent perturbation initial condition  $G_0$  for different pump values  $\mu_1$  from  $\mu_1 = 2.8$  to  $\mu_1 = -18.2$  in steps of 1.5. (b) Numerical delay  $\tau_d$  (circles) and analytical expression  $\tau_d^*$  given by (2) for  $\mu_1 = 2.9$  (dashed). The full line corresponds to a fit of the numerical delays (dashed orange line) with expression (2). (c) Numerical maximum response pulse for  $\mu_1 = 2.9$  (full line) and analytical approximation. In (b) and (c)  $\beta_{sp} = 0$  and  $I(0) = 0.01$ .

laser. In the absence of spontaneous emission ( $\beta_{sp} = 0$ ), the system admits  $\{I = 0\}$  as an invariant manifold. Therefore, any perturbation on the slow variables  $G$  or  $Q$  has no effect and the only way to trigger an excitable pulse is to perturb the laser intensity itself by injecting resonant light into the cavity mode. In order to account for the experimental observations where excitable pulses are produced following an excitation at 800 nm on the gain carrier density, we have introduced a spontaneous emission term  $\beta_{sp}(G + \eta_1)^2$  in the equation for the intensity dynamics. Hence, the steady-state intensity below threshold is not zero anymore and the system is sensitive to perturbations on the pump. It was already shown in Ref. [14] that the excitable threshold decreases linearly with increasing bias pump  $\mu_1$  at lowest order. This result is in good agreement with the experimental observations. Here we analyze the delay in the excitable response using the model of Eqs. (1) for different bias pumps  $\mu_1$ . The results are shown in Fig. 2(a) and reproduce qualitatively well the experimental observations on Fig. 1(b). The delay  $\tau_d$  measures the time difference between the perturbation (considered instantaneous) and the time at the maximum of the excitable response pulse. It diverges for perturbations close to the excitable threshold and saturates for large perturbations. It is also longer for lower bias pump values  $\mu_1$  and for identical perturbation strengths. The agreement with the experimental data is particularly good for high perturbations as expected. Indeed, the presence of noise in the experiment triggers random events that are more likely to occur for perturbations close to the excitable threshold [5]. Those events tend to reduce the effective delay observed with respect to the theoretical expectations. Moreover, this also explains why average delays can be computed for perturbations even below the excitable threshold in Fig. 1(b). The delay between spikes for continuous input stimuli provides a natural coding mechanism called temporal coding [24]. A suprathreshold input stimulus generates a spike with a variable delay and this delay depends on the strength of the input. This coding scheme has been shown to be a plausible mechanism in the visual cortex, as opposed to rate-based coding schemes where the “instantaneous” spiking rate is considered [25].

Analytical expressions have been derived in Ref. [4] for the excitable threshold and the spike latency in the case of equal carrier recombination rates in the gain and in the SA sections. In addition, only coherent perturbations have been

considered, i.e., perturbations on the intensity  $I$ . The same analytical approach cannot be easily extended to the more general case of arbitrary recombination rates  $b_1 \neq b_2$  and of a perturbation on the gain carrier density  $G$  considered here. We have developed another approach using asymptotic methods based on the natural values of the parameters [26,27] to solve this issue. In the case where both the bias pump  $\mu_1$  and the perturbation  $G(0) \equiv G_0$  are close to the first laser threshold  $\mu_{1th} = 1 + \mu_2$ , it is possible to obtain an analytical expression for the spike latency. We use the same definition for this delay as in Ref. [4], i.e., we consider  $\tau_d^*$  as the time needed for the intensity to reach its minimum before growing exponentially fast to large values. This definition of the spike latency thus neglects the pulse duration itself and differs from the one computed in the experiment but allows nevertheless analytic insights. The onset of a successful pulse requires that  $G_0 > G_{0c} \equiv 2\mu_{1th} - \mu_1 - \sqrt{2(b_2\mu_2s - b_1\mu_{1th})I_0}$ , which is slightly below  $2\mu_{1th} - \mu_1$  since  $I_0 \ll 1$ . Note also that since we imposed that  $\mu_{1th}$  is close to  $\mu_1$ , we recover the simple observation that in order to trigger an excitable pulse we need that the net gain  $G - Q - 1$  reaches values close to zero [14]. Of physical interest is the asymptotic limit of the delay  $\tau_d^*$  when  $G_0 - G_{0c} \rightarrow 0^+$ . It takes the form

$$\tau_d^* = \frac{\pi}{\sqrt{2(G_0 - G_{0c})(2\mu_{1th} - \mu_1 - G_{0c})}}, \quad (2)$$

showing an inverse square-root dependence close to the critical perturbation:  $\tau_d^* \sim (G_0 - G_{0c})^{-1/2}$ . This is the typical scaling law for a solution near a saddle point, as it is the case here. Let us remember that  $\tau_d^*$  is the time for the intensity to reach its minimum. It tells us that if  $G_0$  is sufficiently close to  $G_{0c}$ , there is a substantial period of time where the intensity remains low before the onset of the large intensity pulse. If  $G_0 > 2\mu_{1th} - \mu_1$ , then our analysis shows that the intensity grows exponentially immediately without exhibiting a significant prepulse period. In Fig. 2(b), the spike latency  $\tau_d$  is computed numerically with  $\mu_1 = 2.9$  from the full model and is determined as the time the pulse reaches its maximum. It is compared to the expression (2) for  $\tau_d^*$  valid for  $G_0$  close to the critical gain  $G_{0c}$ . The agreement is only qualitative. A better agreement can be reached if one fits the numerically

obtained values with the functional dependence

$$\tau_d = \tau_0 + \frac{\tau_1}{\sqrt{G_0 - G'}} \quad (3)$$

to account for the threshold mismatch between the numerical value and the analytic estimate and the difference in the latency definitions. The full line curve in Fig. 2(b) shows (3) with the values  $\tau_0 = -7.98$ ,  $\tau_1 = 17.71$ , and  $G' = 2.98$ . The agreement with the numerical values is much better, thus the inverse square-root dependence is validated. The dotted curve shows the delay  $\tau_d^*$  for lower bias pump  $\mu_1 = 2.8$  and agrees with previous observations on the fact that the delay increases for lower bias for equal perturbation strengths.

#### IV. CONTROL OF THE RELATIVE REFRACTORY PERIOD

The existence of refractory periods is a key property of excitable systems and is linked to the return of the excitable system to its rest state after a spike has been triggered by an adequate perturbation. In biological neurons, it is well known that it is impossible to trigger an excitable response immediately after an action potential spike has been fired, i.e., during the so-called absolute refractory period. In the regime where a second perturbation occurs much later after the spike, the system is again able to emit a response. However, there is also an intermediate regime where the ability to trigger a second response is strongly affected by the emission of the first, and where the response has therefore a smaller amplitude. This defines the relative refractory period. This phenomenon has been recently evidenced in a micropillar laser with saturable absorber [14]. The main result is reproduced in Fig. 3(a).

The excitable threshold increases with decreasing delay between the two perturbations. This also demonstrates that, contrary to a common belief, the excitable threshold is not a fixed quantity [though the topology of the system of Eqs. (1) remains the same] and depends on the history of the system. This may have fundamental repercussions for applications to neuromorphic processing of information. The model consisting of Eqs. (1) was used to characterize double pulse excitation responses and the result is shown in Figs. 3(b)–3(d). The qualitative agreement between the model on Fig. 3(b) and the experimental results on Fig. 3(a) is excellent. When the second perturbation pulse impinges long after the first excitable pulse has fired, the response is not affected and a second excitable pulse is emitted. When this occurs earlier in a delay such that the carriers did not have enough time to relax to their steady-state values, the response level decreases (relative refractory period) until being completely repressed for a sufficiently small delay time (absolute refractory period). Note also the disappearance of the discontinuous response to the second perturbation, marking the fact that the system is not excitable anymore in this domain. The response also depends crucially on the respective gain and SA recombination timescales. As can be seen from Figs. 3(b)–3(d), an active zone containing gain and SA materials with equal recombination times will have a relative refractory period such that the sooner the second perturbation occurs, the more difficult it is to trigger an excitable response [Fig. 3(c)]. For a slightly faster SA medium [Fig. 3(b)], the excitable threshold first increases with delay (<450 ps) and then decreases again

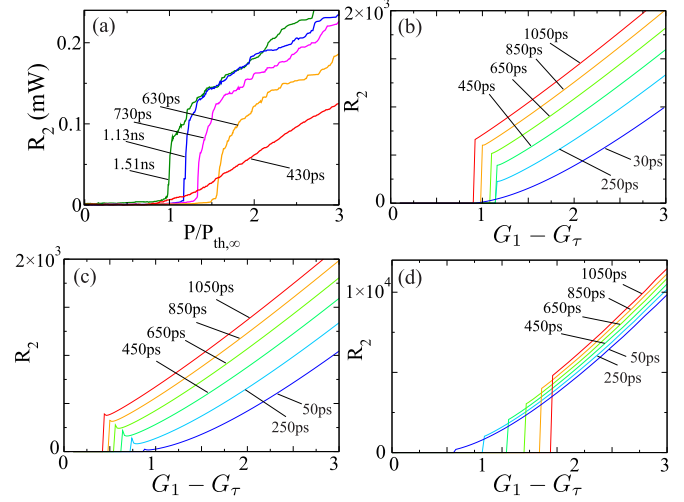


FIG. 3. (a): Experimental measurements of the amplitude of the response  $R_2$  to a second perturbation pulse after an excitable response has been triggered by a first perturbation pulse at  $t = 0$  for different delays between the two perturbations. The perturbation amplitude  $P$  of the second pulse is scaled to the perturbation amplitude at the excitable threshold  $P_{th,\infty}$  for the delay 1.51 ns for which the system has almost completely recovered. [(b)–(d)] Same with the model [Eqs. (1)] and parameters: (b)  $b_1 = 0.001$ ,  $b_2 = 0.002$ ; (c)  $b_1 = 0.001$ ,  $b_2 = 0.001$ ; and (d)  $b_1 = 0.0001$ ,  $b_2 = 0.001$ . In the simulations, a first excitable response is triggered at  $t = 0$  and is followed by a second  $\delta$ -like incoherent perturbation at a variable delay  $\tau$ . The perturbation is characterized by a gain carrier increase  $G(\tau^+) \equiv G_1$  with  $G(\tau^-) \equiv G_\tau$ . The pump parameter is  $\mu_1 = 2.8$  and the other parameters are listed in the text.

for long delays (>450 ps). This case is qualitatively similar to what was observed in the experiment [Fig. 3(a)]. In the case of a very slow gain medium [Fig. 3(d)], the behavior can be reversed: The excitable threshold is smaller for small delays and then increases. This situation is not encountered in standard neurophysiological models. While recovery always occurs for long times, the amplitude of the response is always smaller for small delays. The case  $b_2/b_1 \ll 1$  is not considered since it is not favorable to the excitable regime. In our micropillar laser, we can control to some extent the ratio of recombination rates by changing the temperature of the sample that in turn changes the operating point: For a larger laser threshold, spontaneous recombination of carriers accelerates the gain recombination time and modifies the ratio.

The model also reveals the underlying physical mechanism driving the system response. It shows that the response can be understood simply in terms of the carrier dynamics in the gain and SA zones in very similar terms to those of the case of integrator neurons [28]. Indeed, the second pulse acts as a probe for the gain and carrier dynamical evolution and the system reacts in a manner similar to the static case: Whether a second excitable pulse emission occurs depends on the net gain  $R(t) = G(t) - Q(t) - 1$  as illustrated in Fig. 4. This figure shows different recovery dynamics of the net gain  $R(t)$  after a first excitable pulse has been triggered by a  $\delta$ -like perturbation at time  $t = 0$ . The steady-state value of  $R(t)$  is given by  $\mu_1/(1 + I_{ss}) - \mu_2/(1 + sI_{ss}) - 1$ , with  $I_{ss}$  the steady-state intensity, and is slightly negative. For equal

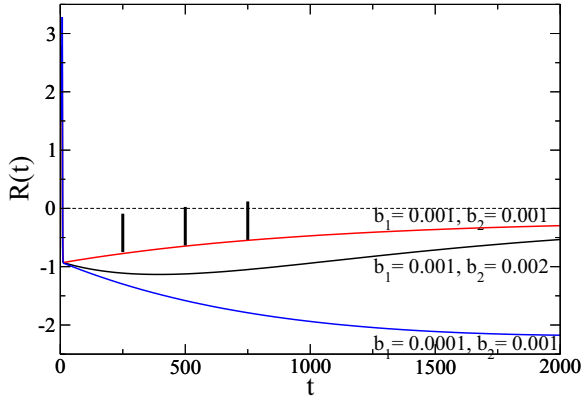


FIG. 4. Net gain  $R(t) = G(t) - Q(t) - 1$  for the same set of parameters as Fig. 3 but different gain and SA recombination rates  $b_{1,2}$  and for an initial excitable pulse triggered at  $t = 0$ . Black vertical thick lines materialize the perturbations on the gain for  $b_1 = 0.001$ .

recombination times in both the gain and the SA sections, the evolution of  $R(t)$  is monotonic and the net gain increases after the excitable pulse has been triggered. Any perturbation on the gain sent to the system will thus trigger a second excitable event if the net gain becomes positive for a sufficiently long amount of time. The excitable threshold will thus decrease for longer delays. The case  $b_2 = 0.002$  is a mixed case since the net gain first decreases and then increases, making the excitable threshold increase for short delays and decrease for longer delays. Finally, for a slow gain medium the excitable threshold initially increases for increasing delays. This matches the decreasing of the net gain and the behavior reverses when the recovery of  $R(t)$  takes place as it starts increasing again (for very long times not shown here).

## V. RESPONSE TO COHERENT AND INCOHERENT PERTURBATIONS

In the previous measurements we only considered perturbations whose wavelength were around 800 nm, i.e., differed from the cavity resonance wavelength. These perturbations are called “incoherent” and their effect is to suddenly increase the gain carrier density, described in the model by a kick in the pump value  $\mu_1$  in Eqs. (1). Since our system contains three relevant physical variables (carrier densities in the SA and gain regions and intracavity intensity,  $Q$ ,  $G$ , and  $I$ , respectively) it could be then perturbed using any of these variables. While perturbations on  $Q$  alone is difficult in our setup since the SA is integrated in the structure and, by design, immune to the input pump [19], it is also possible to perturb the system close to cavity resonance. This kind of perturbation is called “coherent.” By fabrication and depending of the wafer used, the cavity resonance wavelength is in the 980- to 990-nm range. Coherent perturbations are important to demonstrate cascability of the system, a very important point if the output of one micropillar is to be fed to several others (fan-out). It is also the kind of perturbations generally used in models. From an optical processing point of view [13], the possibility to input incoherent perturbations is important for input-output isolation. In this section we investigate the differences between the two types of stimuli.

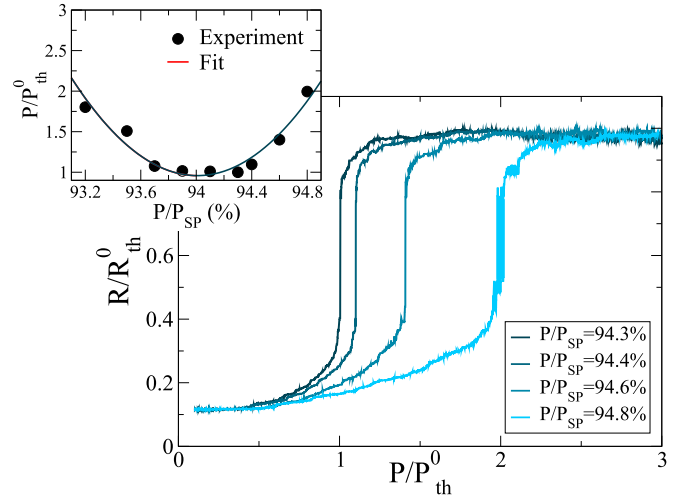


FIG. 5. Left panel: Response amplitude for a coherent perturbation at  $\lambda = 980.47$  nm and different bias pumping with respect to the self-pulsing threshold  $P_{SP}$  pumping value. The response and perturbation amplitudes are scaled to their maximum value for  $P/P_{SP} = 94.3$ . Upper left panel: Excitable threshold dependence for coherent perturbations versus bias pump.

While the excitable behavior is generally defined as producing a response whose amplitude is almost independent from the perturbation that gave rise to it, the excitable response versus perturbation amplitude in Fig. 1 exhibits a linear increase after the sharp jump at the excitable threshold. However, for similar experimental conditions a perturbation acting at cavity resonance (or very close to it) at 980.47 nm will display a marked plateau after the excitable threshold as can be seen on Fig. 5. For different bias pump settings, it is possible to control the excitable threshold as shown on Fig. 1(a). Interestingly, it is shown here that an increase of the bias pump will increase the excitable threshold, at difference with the incoherent case. This is due to the temperature-induced, red detuning of the cavity resonance with increasing pump. The opposite (and “normal”) behavior can be observed for bias pumpings below  $P/P_{SP} = 94.3$ , as is seen in Fig. 5(b). The behavior after the excitable threshold is then a characteristic of the perturbation method. When the perturbation acts on the gain section (incoherent perturbations), the trajectory followed by the system in phase space slightly differs from the trajectory followed in the case of a perturbation on the intensity. However, it is important to note that in each case it is the homoclinic loop that organizes the whole dynamics: There is always a characteristic path followed by the response pulse. A more general definition of the excitable behavior could therefore be the existence of a characteristic, minimal path in phase space that organizes the global dynamics such that there exists a threshold for a small perturbation (smaller than the characteristic size of the path) to trigger a larger excursion.

In order to analyze more deeply the impact of the perturbation type on the trajectory in phase space, we have computed the response of the system for different perturbations mixing perturbations on the gain and on the intensity. More specifically, we have integrated Eqs. (1) with a bias pump  $\mu_1 = 1.5$  and initial conditions  $\{G, Q, I\}(t = 0) = \{G_0, Q_0 = \mu_2, I_0\}$

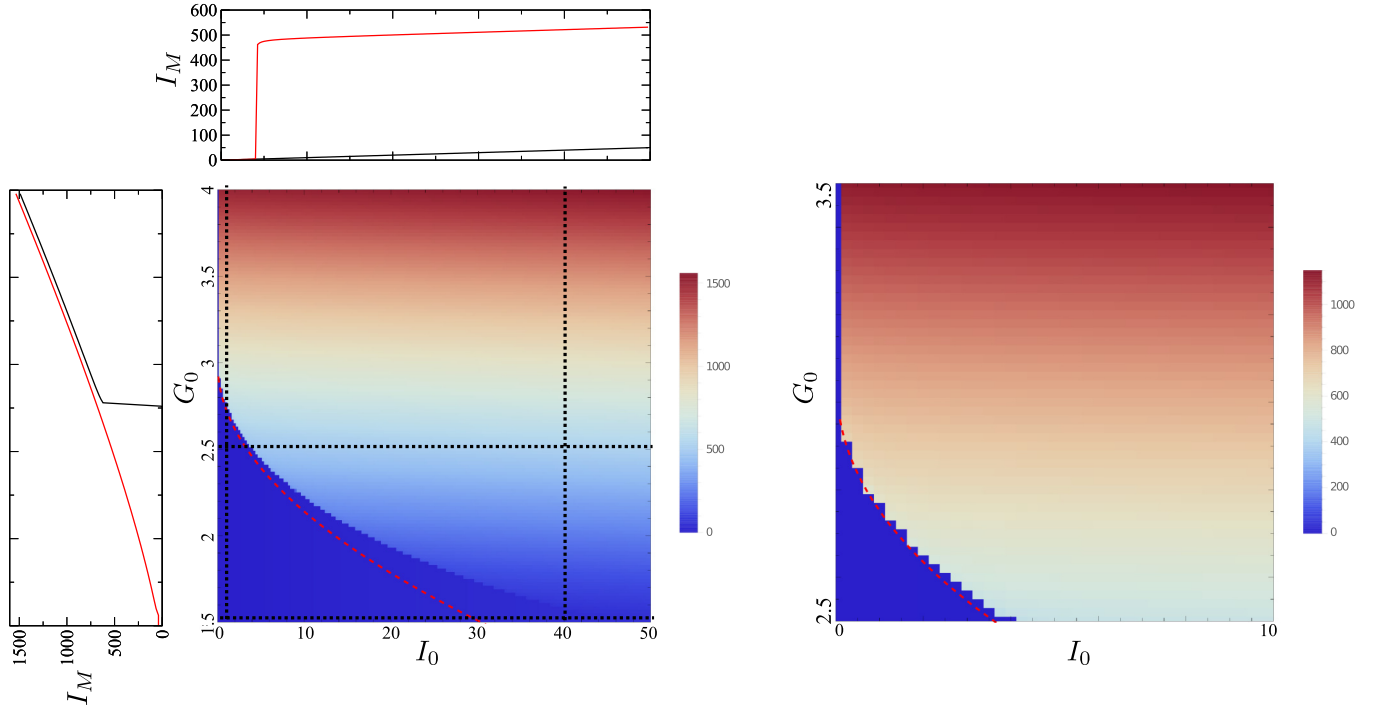


FIG. 6. Maximum intensity  $I_M$  of the response pulse to a mixed perturbation characterized by initial conditions at  $0^+$  for  $\{I, G, Q\}: I_0, G_0, Q_0 = \mu_2$ . Left:  $\mu_1 = 1.5$ . Right: Zoom for  $I_0$  small and  $G_0$  close to the threshold value. Parameters are the one given in the text except  $\beta_{sp} = 0$ . Dashed lines: Analytic formula for the excitable threshold Eq. (4). Sections of the surface are marked by black dotted lines and shown in the side panels for  $G_0 = 1.5, G_0 = 3.5, I_0 = 1, I_0 = 40$ .

and plotted the result in Fig. 6. The lower-left corner represents the set of all subthreshold perturbations [we consider here only positive perturbations ( $G_0 > \mu_1, I_0 > 0$ )]. The excitable threshold is materialized by an abrupt transition in the response amplitude, which demonstrates the excitable character. In the experimental results presented in Figs. 1 and 5, “coherent” perturbations refer to those on the intensity alone  $\{G_0 = \mu_1, I_0\}$  while “incoherent” perturbations refer to those on the gain alone  $\{G_0, I_0 = I_{ss}\}$ . Any other perturbation would then correspond to a linear superposition of these two cases. Above the excitable threshold, the peak intensity grows linearly for perturbations with increasing incoherent part and is almost constant for perturbations with increasing coherent part. Since we chose  $\beta_{sp} = 0$ , there is a singular vertical line of initial conditions  $\{I_0 = 0\}$ , which is under the excitable threshold for any incoherent perturbation amplitude. For any small intensity, however ( $G_0, I_0 > 0$ ), the singularity disappears. For  $G_0 = \mu_1$  corresponding to purely coherent perturbations, the only steady-state point is the laser-off state and the system is no longer excitable (the system is below the saddle-node bifurcation point S in Fig. 2 of Ref. [4]), as is visible in Fig. 6. Similarly, for  $I_0 \gg 40$ , the system no longer exhibits an abrupt transition for an increasing perturbation on gain but instead displays a rather smooth transition, characteristic of a gain-switching regime. This regime transition was experimentally demonstrated in Ref. [14]. Note that the amplitude of the response in the case of coherent perturbations depends also on the bias pump  $\mu_1$ , while being almost insensitive to the strength of the coherent perturbation amplitude: The response is larger for larger pump intensities. It is possible to find an analytical expression for the excitable threshold in the case of

a perturbation on the gain, arbitrary recombination rates in the gain and in the SA,  $\mu_1 \lesssim \mu_{1th}$  and for  $\beta_{sp} = 0$  [27]. The critical perturbation on the gain at the excitable threshold reads

$$G_{0c} = \mu_{1th} + \sqrt{2b_1(\mu_{1th} - \mu_1) \left[ \ln \left( \frac{I_s}{I_0} \right) - \frac{(I_s - I_0)}{I_s} \right]}, \quad (4)$$

where

$$I_s = \frac{\mu_1 - \mu_{1th}}{\mu_{1th} - (b_2/b_1)\mu_{2s}} > 0 \quad (5)$$

and  $I_0 = I(0) \ll 1$ . Since  $\mu_1 < \mu_{1th}$ , the inequality  $I_s > 0$  requires that  $\mu_{1th} - (b_2/b_1)\mu_{2s} < 0$ , which corresponds to the condition for a subcritical steady bifurcation at threshold only if  $b_2 = b_1$ . If  $b_2 \neq b_1$ , then (5) depends on the ratio  $b_2/b_1$  and results from the fact that we are dealing with a dynamical phenomenon and not a steady state. The condition  $\mu_{1th} - (b_2/b_1)\mu_{2s} < 0$  is thus a necessary condition for excitability. The result is plotted in Fig. 6. The agreement is good even for a relatively large initial intensity value  $I_0$ . Given the fact that  $b_1 \ll 1$ , it is clear that in first approximation the excitable threshold is linearly controlled by the value of the bias pump  $\mu_1$  since  $G_{0c} \simeq \mu_{1th} \simeq \mu_1$ .

Physically, the suprathreshold behavior of the excitable response amplitude can be explained by the fact that in the incoherent perturbation case, the perturbation acts on the gain and therefore the gain increases just after the perturbation, giving rise to an increased response, whereas for a coherent perturbation the gain is not immediately affected by the

perturbation. It is affected afterwards, through the nonlinear dynamics, making the response amplitude rather independent of the perturbation amplitude. This also explains why the amplitude of the response differs for increasing coherent perturbation amplitudes but fixed incoherent ones. On a more theoretical level, the homoclinic bifurcation giving rise to the excitable property necessitates a phase space of dimension greater than two (three here), as compared to the dynamics of, e.g., the saddle-node on invariant circle bifurcation that takes place in one dimension and for which the excitable response amplitude is necessarily clamped.

A more quantitative argument can be given by considering the high-intensity limit of the set of Eqs. (1). In this limit the equations read (with  $\beta_{sp} = 0$ )

$$\begin{aligned} \dot{I} &= (G - Q - 1)I \\ \dot{G} &= -b_1GI \\ \dot{Q} &= -b_2sQI. \end{aligned} \quad (6)$$

These equations are boundary layer (or inner layer) equations which must be solved with the matching conditions  $b_1I \rightarrow I_0$ ,  $G \rightarrow G_0$ , and  $Q \rightarrow \mu_2$  as  $t \rightarrow -\infty$ . Dividing the equation for  $Q$  by the one for  $G$ , one can integrate the system that leads to  $Q = \mu_2(G/G_0)^m$  with  $m = sb_2/b_1$  and  $G_0 = \mu_1$  for a coherent perturbation and  $G_0 > \mu_1$  for an incoherent one. By reporting the result in the equation for  $I$  and dividing by the equation for  $G$ , one can integrate the system to get (with  $I_0 \ll I$ )

$$I = \frac{1}{b_1} \left\{ \ln \left( \frac{G}{G_0} \right) - (G - G_0) + \frac{\mu_2}{m} \left[ \left( \frac{G}{G_0} \right)^m - 1 \right] \right\}. \quad (7)$$

Just after the high-intensity pulse, the systems sets in its saturated phase with  $I \rightarrow 0$ ,  $G \rightarrow G_a$ , and  $Q \rightarrow Q_a$ . Assuming  $G_a/G_0 < 1$  and since  $m$  is numerically large, we find  $G_a \simeq G_0 \exp(-G_0)$ . We are interested in the maximum intensity which appears at  $G = G_M$  and satisfying  $G - \mu_2(G/G_0)^m = 1$  or, since  $m$  is large,  $G_M \simeq 1$ . Inserting the latter into (7), we obtain finally the maximum pulse intensity  $I_M$  as

$$I_M \simeq \frac{1}{b_1} \left[ \ln \left( \frac{1}{G_0} \right) - (1 - G_0) + \frac{\mu_2}{m} \right]. \quad (8)$$

This expression tells us that for a coherent perturbation, the maximum intensity reached by the excitable pulse does not depend in first approximation on the coherent perturbation since in that case  $G_0$  is always equal to  $\mu_1$ . On the contrary, for a perturbation on the gain one has  $G_0 > \mu_1$ , which obviously depends on the perturbation strength and leads to a dependence of  $I_M$  on  $G_0$ . A comparison of the analytic approximation (8) and of the solution from the numerical simulation of the full model is shown in Fig. 2(c). The agreement is very good.

Another interesting aspect for practical applications lies in the perturbation energy necessary to elicit a response. For the same micropillar illuminated by coherent and incoherent perturbations, the excitable threshold energy for incoming pulses on the micropillar is measured respectively to be 3.75 fJ and 725 fJ. This is to be compared to the response pulse energy at threshold which is of the order of 50 fJ. Since the

perturbation pulse is measured without taking into account the mode matching of the input pulse to the micropillar, its value is overestimated but remains much smaller than the perturbation in the coherent case. In the incoherent case, the same restrictions apply, in addition to the fact that the perturbation acts at  $\sim 800$  nm and not directly on the field at 980 nm, leading to a different dynamics as already mentioned. Additional losses are also present, for instance, the quantum defect between the perturbation energy and the energy gap of the wells. A direct comparison of the perturbation pulse energy to the response pulse energy is therefore meaningless in such a case.

## VI. CONCLUSION AND PERSPECTIVES

In conclusion, we have provided a detailed analysis of the nonlinear timing and response properties of an excitable micropillar laser with saturable absorber experimentally, numerically, and, whenever possible, analytically. The nonlinear latency in the response has been investigated and shown to provide a natural nonlinear coding mechanism in the framework of neuromimetic systems called temporal coding. This coding scheme seems promising for mimicking some biological mechanisms of visual perception with a substantial gain in the time scales at stake ( $> 10^6$ ). We have provided a physical explanation of the different behaviors observed during the relative refractory period as a function of the recombination rates in the gain and saturable absorber sections in terms of a dynamical change in the net gain. We have investigated the coherent and incoherent perturbation techniques. The former gives rise to an above-threshold response amplitude that depends weakly on the incoming stimulus, as generally expected in an excitable system, whereas the latter shows a linear dependence. In both cases, however, the response amplitude depends on the bias pump. We have provided an explanation for such a behavior and provided a more general definition of an excitable behavior. Analytic expressions obtained with singular perturbation techniques have allowed us to assess the observed behaviors. At last, we have measured excitable threshold pulse energies as low as a few femtojoules with typical responses in the 50-fJ range, in line with current low-consumption devices in the range of 1 fJ/bit [29]. While this does not account for the bias pumping energy, this result is encouraging in view of using such devices as elements of an efficient photonic platform for artificial neural networks and neuro-inspired computing. Given the small footprint of micropillar lasers, they can be coupled to form networks either by free-space optics, using more advanced arrangements (e.g., a spatial light modulator as in Ref. [30]), or by evanescent coupling [31]. These networks could then be used to demonstrate neuromimetic functionalities such as theoretically studied in Ref. [7].

## ACKNOWLEDGMENTS

The authors acknowledge partial support from the French Renatech network. T.E. acknowledges the support of the Fonds National de la Recherche Scientifique (Belgium) and the Belgian Science Policy Office under Grant No. IAP-7/35 “photonics@be.”

- [1] F. Plaza, M. G. Velarde, F. T. Arecchi, S. Boccaletti, M. Ciofini, and R. Meucci, *Europhys. Lett.* **38**, 85 (1997).
- [2] A. M. Yacomotti, M. C. Eguia, J. Aliaga, O. E. Martinez, G. B. Mindlin, and A. Lipsich, *Phys. Rev. Lett.* **83**, 292 (1999).
- [3] J. L. A. Dubbeldam and B. Krauskopf, *Opt. Commun.* **159**, 325 (1999).
- [4] J. L. A. Dubbeldam, B. Krauskopf, and D. Lenstra, *Phys. Rev. E* **60**, 6580 (1999).
- [5] S. Barbay, R. Kuszelewicz, and A. M. Yacomotti, *Opt. Lett.* **36**, 4476 (2011).
- [6] A. Jacobo, D. Gomila, M. A. Matias, and P. Colet, *New J. Phys.* **14**, 013040 (2012).
- [7] A. N. Tait, M. A. Nahmias, Y. Tian, B. J. Shastri, and P. R. Prucnal, in *Nanophotonic Information Physics*, edited by M. Naruse (Springer, Berlin, 2014), pp. 183–222.
- [8] P. R. Prucnal, B. J. Shastri, T. F. de Lima, M. A. Nahmias, and A. N. Tait, *Adv. Opt. Photon.* **8**, 228 (2016).
- [9] M. Nahmias, B. Shastri, A. Tait, and P. Prucnal, *IEEE J. Sel. Top. Quantum Electron.* **19**, 1 (2013).
- [10] B. Garbin, J. Javaloyes, G. Tissoni, and S. Barland, *Nat. Commun.* **6**, 5915 (2015).
- [11] B. J. Shastri, A. N. Tait, M. Nahmias, B. Wu, and P. Prucnal, in *CLEO: 2014* (Optical Society of America, San Jose, CA, 2014), p. STu3I.5.
- [12] F. Selmi, R. Braive, G. Beaudoin, I. Sagnes, R. Kuszelewicz, and S. Barbay, *Opt. Lett.* **40**, 5690 (2015).
- [13] B. J. Shastri, M. A. Nahmias, A. N. Tait, A. W. Rodriguez, B. Wu, and P. R. Prucnal, *Sci. Rep.* **6**, 19126 (2016).
- [14] F. Selmi, R. Braive, G. Beaudoin, I. Sagnes, R. Kuszelewicz, and S. Barbay, *Phys. Rev. Lett.* **112**, 183902 (2014).
- [15] W. M. Kistler and W. Gerstner, *Neur. Comput.* **14**, 987 (2002).
- [16] S. Thorpe, A. Delorme, and R. Van Rullen, *Neur. Netw.* **14**, 715 (2001).
- [17] T. Gollisch and M. Meister, *Science* **319**, 1108 (2008).
- [18] T. Elsass, K. Gauthron, G. Beaudoin, I. Sagnes, R. Kuszelewicz, and S. Barbay, *Appl. Phys. B* **98**, 327 (2010).
- [19] T. Elsass, K. Gauthron, G. Beaudoin, I. Sagnes, R. Kuszelewicz, and S. Barbay, *Eur. Phys. J. D* **59**, 91 (2010).
- [20] T. J. Gawne, T. W. Kjaer, and B. J. Richmond, *J. Neurophysiol.* **76**, 1356 (1996).
- [21] M. Yamada, *IEEE J. Quantum Electron.* **29**, 1330 (1993).
- [22] F. Prati, P. Caccia, G. Tissoni, L. Lugiato, K. Mahmoud Aghdami, and H. Tajalli, *Appl. Phys. B* **88**, 405 (2007).
- [23] E. Izhikevich, *IEEE Trans. Neur. Netw.* **15**, 1063 (2004).
- [24] P. Dayan and L. Abbott, *Theoretical Neuroscience: Computational and Mathematical Modeling of Neural Systems*, Computational Neuroscience Series (Massachusetts Institute of Technology Press, Cambridge, MA, 2001).
- [25] S. J. Thorpe, in *Parallel Processing in Neural Systems and Computers*, edited by R. Eckmiller, G. Hartmann, and G. Hauske (North-Holland Elsevier, Amsterdam, 1990), p. 91.
- [26] T. Erneux and P. Glorieux, *Laser Dynamics* (Cambridge University Press, Cambridge UK, 2010).
- [27] T. Erneux and S. Barbay (unpublished).
- [28] E. M. Izhikevich, *Neur. Netw.* **14**, 883 (2001).
- [29] D. A. Miller, *Proc. IEEE* **97**, 1166 (2009).
- [30] D. Brunner and I. Fischer, *Opt. Lett.* **40**, 3854 (2015).
- [31] F. Selmi, Ph.D. thesis, Université Paris Sud, Paris XI (2015).